

Processing effects on the magnetic and mechanical properties of FeCoNiAl_{0.2}Si_{0.2} high entropy alloy

Ting-ting Zuo¹⁾, Song-bo Ren²⁾, Peter K. Liaw³⁾, and Yong Zhang¹⁾

1) State Key Laboratory for Advanced Metals and Materials, University of Science and Technology Beijing, Beijing 100083, China

2) Beijing Hangke Engine Control System Science & Technology Co., Ltd., Beijing 102200, China

3) Department of Materials Science and Engineering, The University of Tennessee, Knoxville TN 37996, USA

(Received: 13 August 2012; revised: 25 September 2012; accepted: 5 October 2012)

Abstract: High entropy alloys with the composition of FeCoNiAl_{0.2}Si_{0.2} were prepared by arc melting and induction melting, denoted by A1 and A2, respectively. The samples prepared by these two techniques have a face-centered cubic (FCC) phase structure and a typical dendrite morphology. The tensile yield strength and maximum strength of A2 samples are about 280 and 632 MPa, respectively. Moreover, the elongation can reach 41.7%. These two alloys prepared by the different methods possess the similar magnetic properties. The saturation magnetization and coercivity can reach 1.151 T and 1400 A/m for A1 samples and 1.015 T and 1431 A/m for A2 samples, respectively. Phases in A2 samples do not change, which are heat treated at different temperatures, then quenched in water. Only the sample, which is heat treated at 600°C for 3 h and then furnace cooled, has a new phase precipitated. Besides, the coercivity decreases obviously at this temperature. Cold rolling and the subsequent heat treatment cannot improve the magnetic properties effectively. However, cold rolling plays an important role in improving the strength.

Keywords: high entropy alloys; magnetic properties; mechanical properties; heat treatment

1. Introduction

Recently, high entropy alloys (HEAs) have received the considerable attention to be used in aerospace and other special areas because of their high strength, good oxidation resistance, excellent high-temperature stability, and so on [1-7]. For conventional alloys, there are usually one or two dominated elements in them [8]. However, HEAs jump out of this design concept. They usually contain more than five elements, each of these contents is more than 5% by atom number, and there is no dominant element [9]. Because of the special design, certain effects called 'high entropy', 'sluggish-diffusion', 'lattice distortion', and 'cocktail' effects are observed in HEAs [10]. According to the maximum entropy-production principle (MEPP) [11], high entropy intends to stabilize high-entropy phases, such as amorphous phases and solid-solution phases, rather than intermetallic phases. Efforts have been made to find a simple guideline for the design of these complex alloys. For example, Zhang *et al.* [12] formulated rules for the for-

mation of HEAs, which were further simplified by Yang *et al.* [13] through proposing a parameter. Guo *et al.* [14] correlated the stability of face-centered cubic (FCC) and body-centered cubic (BCC) solid solutions with the valence electron concentration (VEC). Besides the thermodynamic factors, the dynamic preparation process also influences the phase formation [15-18]. The HEAs exhibit the very interesting properties of high strength, high hardness, and excellent high-temperature stability, which improve the abrasion performance, corrosion resistance, high electrical resistivity, and so on [4, 19-25].

The history of HEAs is relatively short and has been principally focused on their mechanical properties [3, 5, 26-27]. Little effort is made on the magnetic properties. Wang *et al.* [28] studied the magnetic properties of CoCrCuFeNiTi_x alloys. The FCC solid solutions forming in CoCrCuFeNi and CoCrCuFeNiTi_{0.5} alloys exhibited the typical paramagnetism, whereas CoCrCuFeNiTi_{0.8} and CoCrCuFeNiTi showed the superparamagnetism, which

Corresponding author: Yong Zhang E-mail: drzhangy@ustb.edu.cn

was attributable to the embedding of nanoparticle assemblies in the amorphous phase with the addition of Ti. Kao *et al.* [4] found that the magnetic properties of as-homogenized CoCrFeNiAl_x alloys were associated with the crystal structure and Al/AlNi-rich phase. In this work, a new magnetic $\text{FeCoNiAl}_{0.2}\text{Si}_{0.2}$ HEA was designed and studied by measuring its resistivity, magnetization, and strength. Heat treatment and cold rolling were used to improve its properties. The relevant parameters obtained by these methods were compared to provide the insight concerning the comprehensive performance of this alloy.

2. Experiment procedures

Button ingots (A1) with the nominal compositions of $\text{FeCoNiAl}_{0.2}\text{Si}_{0.2}$ were prepared by arc melting from pure elements with the purity higher than 99.5wt% in high-purity argon atmosphere on a water-cooled Cu hearth. The alloys were remelted four times to improve their homogeneity. For convenience, a large ingot (A2) with the same composition was prepared by induction melting. The crystal structures were identified using an X-ray diffractometer under the radiation conditions of 30 kV, 20 mA, a Cu target, and a scanning speed of $10^\circ/\text{min}$. Transmission electron microscopy (TEM) was used to verify the structures. Compressive tests of the cylindrical samples with the dimension of $\phi 3 \text{ mm} \times 6 \text{ mm}$ were investigated using an MTS 809 materials testing machine at room temperature with a strain rate of $2 \times 10^{-4} \text{ s}^{-1}$. The tensile tests were conducted on a CMT4105 materials testing machine under a strain rate of $5 \times 10^{-4} \text{ s}^{-1}$ at room temperature. The microstructures of cross-sections were examined using a ZEISS SUPRA 55 field emission scanning electron microscope (SEM) with energy dispersive spectrometry (EDS) and a ZEISS UMT200i metallographic microscope. The magnetization curves were obtained by using the instrument of "Physical Property Measurement System" (PPMS) made by American Quantum Design Company. The electrical resistivity was measured using a precise resistance tester AT510. A2 samples were heat treated at different temperatures (500, 600, 700, 800, 900, and 1000°C) for 3 h. Then, one sample was quenched in water, and the other one was furnace cooled from each temperature. The cold rolling of A2 samples was cut from the radial direction of the ingot and then cold rolled for 60% reduction with each reduction in pass of 0.1 mm. Finally, the as-rolled samples were annealed at 900°C for 4 h and furnace cooled.

3. Results and discussion

3.1. Microstructure

Fig. 1 shows the X-ray diffraction (XRD) patterns of

the alloys prepared by different methods. Both kinds of alloys have the similar FCC structure. By identifying the highest peaks, the calculated lattice constants are 0.35708 (A1) and 0.35944 nm (A2), respectively. According to Guo *et al.* [14], the FCC stable region is $\text{VEC} > 8$. The calculated VEC of the alloys in this study is 8.353, which agrees well with the model. These two alloys have the typical cast dendritic and interdendritic structures (simplified as DR and ID), as shown in Fig. 2. The dendritic area (DR) is rich in Fe and Co, while the interdendritic area (ID) is rich in Al, Ni, and Si. This may be attributed to the low melting point of Al and more negative high enthalpy of mixing between Si and Ni. In addition, the interdendritic area of A1 alloy is more obvious than that of A2 alloy. This may be due to the different processing of the alloys. For A2 alloy (induction melted), the elements are mixed more uniformly with electromagnetic stirring. Therefore, little segregation can be found in A2 alloy, and the contrast between DR and ID is not so obvious. The bright-field TEM image of the arc melted HEA shows the existence of particles in the dendritic area with the diameter of $\sim 2 \mu\text{m}$ in Fig. 3(a). The [001] zone axis diffraction pattern in Fig. 3(b) displays superlattice reflections generated by the particle precipitates, indicating the existence of ordered BCC phases. This may be confirmed by the minor peak in Fig. 1(a) at $2\theta \approx 25^\circ$. Due to the relatively small amount of such particles, their diffraction peaks are very low. Similar reports of the ordered phases can also be found [22, 29]. Aside from this, some BCC region can also be found around the particles as shown in Fig. 3(c), which has a faint hint in the XRD pattern at about $2\theta \approx 45^\circ$. Further study is necessary to give quantitative information on the relative amount of disordered or ordered phases in HEAs.

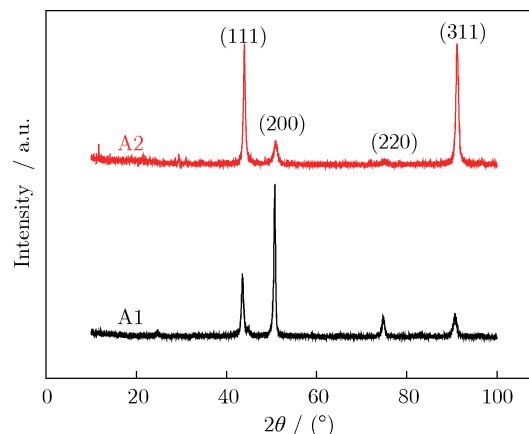


Fig. 1. XRD patterns of the $\text{FeCoNiAl}_{0.2}\text{Si}_{0.2}$ alloys prepared by arc melting (A1) and induction melting (A2).

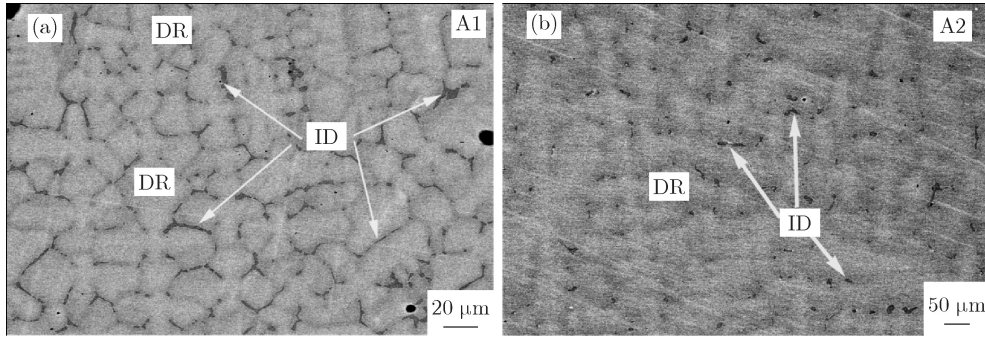


Fig. 2. Back scanning electron images of FeCoNiAl_{0.2}Si_{0.2} alloys prepared by two methods: (a) arc melting; (b) induction melting.

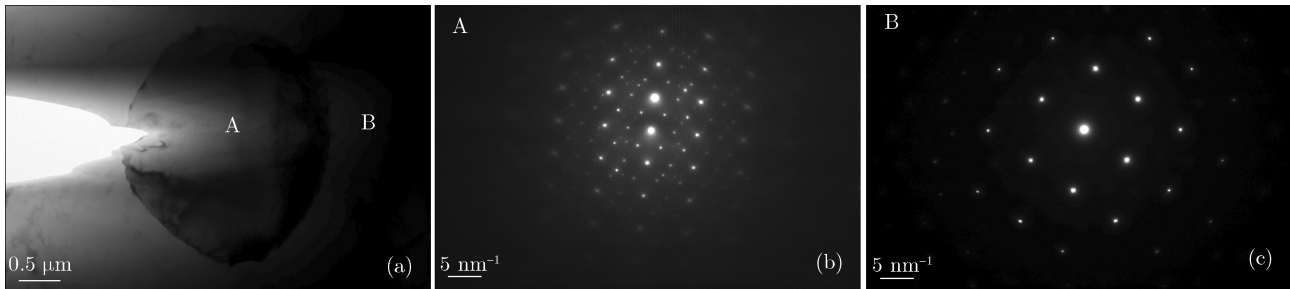


Fig. 3. TEM bright-field image of A1 sample (a), electron diffraction pattern of the particle in (a) from the [001] zone axis (b), and electron diffraction pattern of the outside region beside the particle (c).

In Fig.4, the XRD patterns of A2 samples after quenching also exhibit the same FCC structure, indicating the good high-temperature phase stability. High cooling rate may freeze the high-temperature phase structure and avoid the other phase separating out. However, after furnace cooling, only the sample annealed at 600°C shows a different XRD pattern. This trend may indicate some phase precipitations forming at this temperature. A

similar phenomenon can also be found in the annealed Al_{0.5}CoCrCuFeNi alloy [30]. The phase precipitations may relate to the ordering process of the disordered solid solution during the long time holding at specific temperature. While for the sample annealed at 600°C with water quenching, no phase precipitation can be observed, and this probably indicates that the ordering process needs a slower cooling to happen.

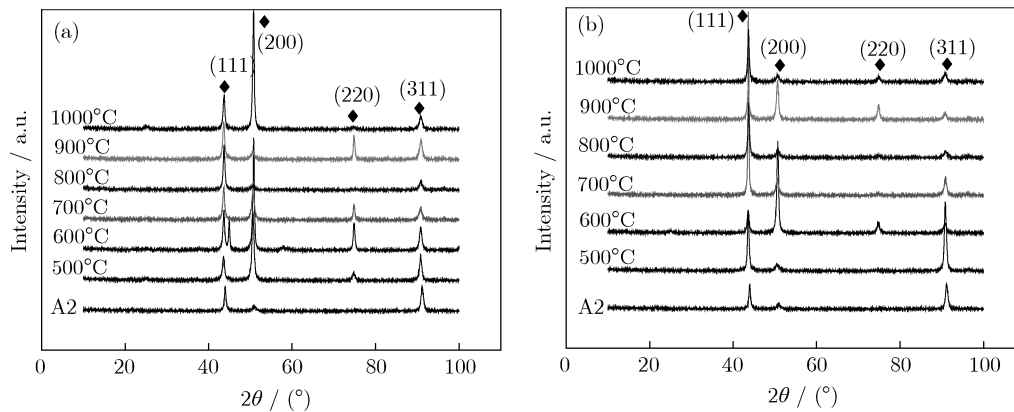


Fig. 4. XRD patterns of A2 samples after different heat treatments: (a) furnace cooling; (b) water quenching.

3.2. Mechanical properties

Fig. 5(a) presents the room-temperature compressive engineering stress-strain curves of the alloys prepared by

two different methods. They all exhibit the good plasticity and significant work hardening, which may be due to the solid-solution strengthening effect caused by adding the small atomic size element, Si, and large atomic size ele-

ment, Al. The plastic deformation can reach 50% without fracture for both samples. The compressive yield strength is about 342 MPa for A1 sample and 291 MPa for A2 sample. Fig. 5(b) shows the room-temperature tensile engineering stress-strain curves of A2 alloy. The yield strength and maximum strength are about 280 and 636 MPa, respectively. The elongation can reach 41.6%. The tensile yield strength is a little lower than the compression yield strength, which may be due to the fact that the tensile is more sensitive to defects. Fig. 6 shows the SEM images of the fracture surface and lateral face morphology of A2 sample after tensile test. The angle between the fracture

surface and horizontal axial is 30° . Many slip bands can be found at the lateral face. Dimples can be clearly seen in Figs. 6(c) and (d), indicating a ductile fracture. After cold rolling, the yield strength increases to 1149 MPa, and the plasticity decreases by $\sim 4\%$ in Fig. 5(b). Fig. 7 shows the fracture morphology after tensile test. The angle between the fracture surface and horizontal axial is 20° . Tearing dimples and some small holes can be seen on the surface. This indicates that the fracture mechanism is porous aggregation fracture [31]. Besides, many slip bands are located on the lateral surface.

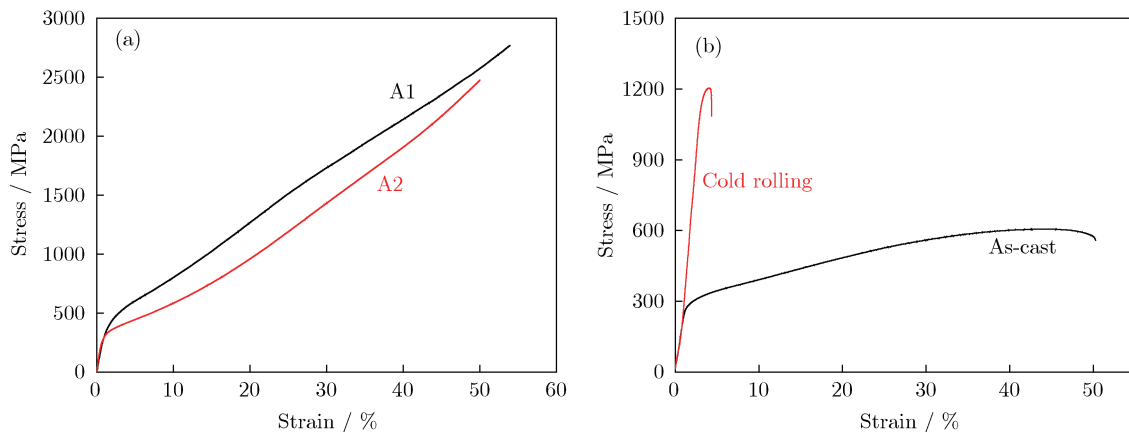


Fig. 5. Compressive engineering stress-strain curves of $\text{FeCoNiAl}_{0.2}\text{Si}_{0.2}$ alloys (a) and tensile engineering stress-strain curves of the induction melted $\text{FeCoNiAl}_{0.2}\text{Si}_{0.2}$ alloy (b).

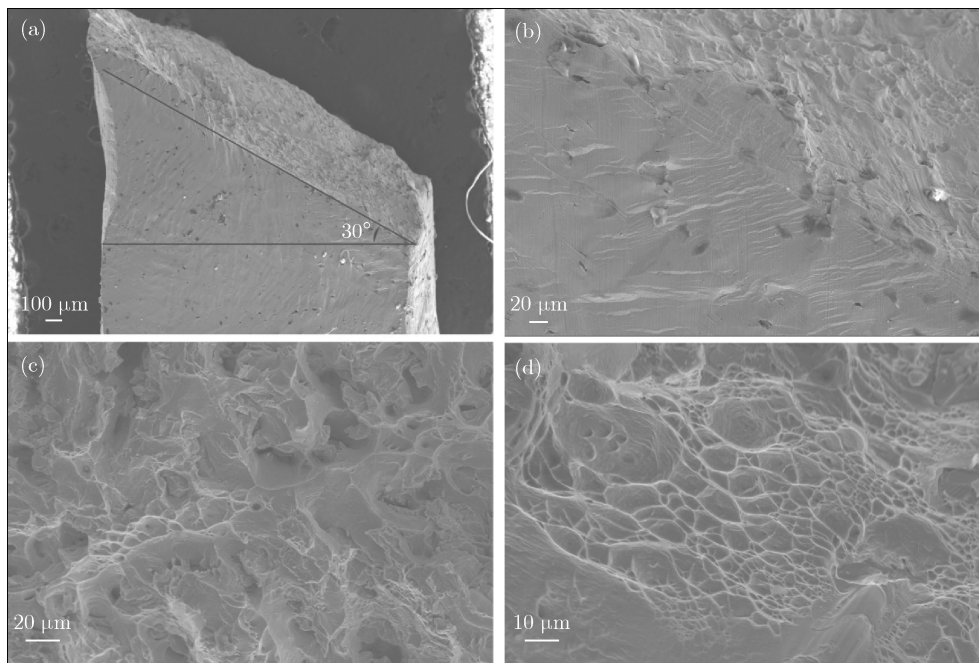


Fig. 6. SEM images of the lateral surface ((a) and (b)) and fracture surface ((c) and (d)) of the induction melted $\text{FeCoNiAl}_{0.2}\text{Si}_{0.2}$ alloy after tensile deformation at room temperature.

3.3. Magnetic properties

Hysteresis loops measured for FeCoNiAl_{0.2}Si_{0.2} alloys at room temperature are shown in Fig. 8. The saturation magnetization (M_s), coercivity (H_c), and remnant magnetism (M_r) of both alloys determined from the loops are listed in Table 1. It is clear that the induction melted alloy

has the similar magnetic properties to the arc melted one. The saturation magnetization and coercivity can reach 1.151 T and 1400 A/m for A1 sample and 1.015 T and 1431 A/m for A2 sample. The electrical resistivity of A1 sample is 69.5 $\mu\Omega\cdot\text{cm}$. The little decrease of M_s for A2 sample may be related to the casting defects.

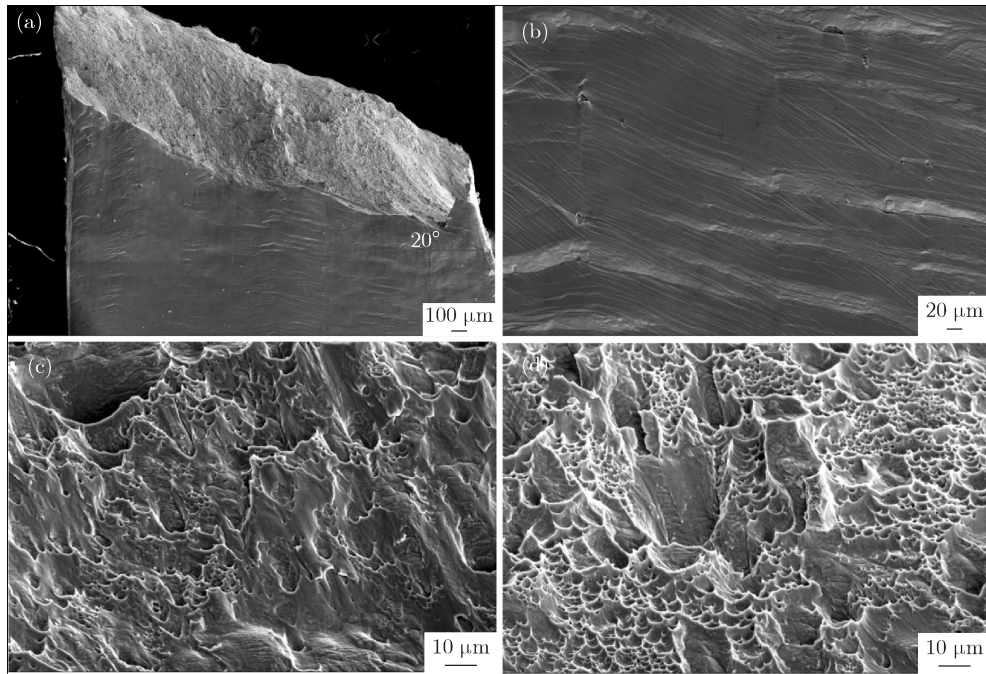


Fig. 7. SEM images of the lateral surface ((a) and (b)) and fracture surface ((c) and (d)) of the cold-rolled induction-melted FeCoNiAl_{0.2}Si_{0.2} alloy after tensile deformation at room temperature.

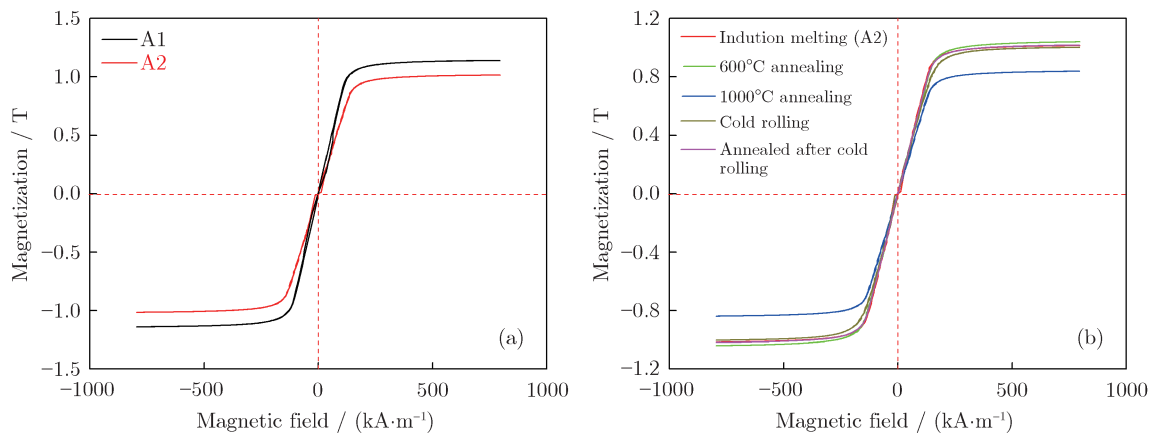


Fig. 8. Magnetic properties of the FeCoNiAl_{0.2}Si_{0.2} alloys: (a) hysteresis loops of the alloy prepared by two methods; (b) hysteresis loops of A2 samples after different processes.

It is well known that soft magnetic materials are often characterized by high saturation magnetization, high magnetic susceptibility, and high electrical resistivity, as well as low coercivity. Although the value of coercivity in this study is somewhat higher, it is not unusual for the as-cast alloy without the subsequent heat treatment. The

saturation magnetization is primarily determined by the composition and crystal structure but less sensitive to the microstructures, such as the grain size and morphology. In contrast, the coercivity, which is inversely proportional to the permeability, is affected by the grain size, stress, impurity, deformation, and the subsequent heat-treatment pro-

cess [32]. Therefore, after annealing at 600°C and 1000°C for 3 h, the coercivity of A2 samples decreases largely, from 1431 A/m to 693 A/m and 807 A/m, respectively. This trend may be ascribed to the releasing of internal stress. The texture can also improve the magnetic properties. Moreover, one technique to produce the texture is repeatedly cold rolling and heat treatment [33]. To our surprise, the magnetic properties of A2 alloy are not improved after cold rolling and heat treatment. This trend may be due to the fact that the optimal texture does not form after these treatment processes, or the optimal magnetic axis is not in the rolling direction.

Table 1. Magnetic properties of FeCoNiAl_{0.2}Si_{0.2} HEAs

Processing	M_s / T	H_c / (A·m ⁻¹)	M_r / T
Arc melting	1.151	1400.720	0.01163
Induction melting	1.015	1431.430	0.00539
Cold rolling	1.003	1437.786	0.00903
Annealed at 900°C after cold rolling	1.018	1508.325	0.00785
Annealed at 600°C	1.040	696.531	0.00392
Annealed at 1000°C	0.838	807.593	0.00388

4. Conclusions

FeCoNiAl_{0.2}Si_{0.2} HEAs prepared by arc melting and induction melting have the same FCC structure. These alloys have the similar excellent over-all properties, such as good plasticity and high magnetic saturation. The general properties of A1 sample are slightly better. The compressive yield strength can reach 342 MPa for A1 alloy and 291 MPa for A2 alloy. The magnetic saturation and coercivity are 1.15 T and 1400 A/m for A1 sample, and 1.015 T and 1431 A/m for A2 sample, respectively. The electrical resistivity of A1 sample is 69.5 μΩ·cm. TEM results show the ordered BCC particles and BCC phase in the arc melted sample. Annealing at different temperatures has not changed the phases largely. Only A2 sample, which is heat treated at 600°C and then furnace cooled, has a new phase precipitation, and its coercivity decreases largely. Cold rolling for A2 sample increases the yield strength to 1149 MPa, but decreases the plasticity. The selected cold rolling for 60% reduction and the following heat treatment have not improved the magnetic properties largely.

References

- [1] J.W. Yeh, S.K. Chen, S.J. Lin, J.Y. Gan, T.S. Chin, T.T. Shun, C.H. Tsau, and S.Y. Chang, Nanostructured high-entropy alloys with multiple principal elements: novel alloy design concepts and outcomes, *Adv. Eng. Mater.*, 6(2004), No. 5, p. 299.
- [2] Y.F. Kao, T.J. Chen, S.K. Chen, and J.W. Yeh, Microstructure and mechanical property of as-cast, -homogenized, and -deformed Al_xCoCrFeNi (0 ≤ x ≤ 2) high-entropy alloys, *J. Alloys Compd.*, 488(2009), p. 57.
- [3] Y.J. Zhou, Y. Zhang, T.N. Kim, and G.L. Chen, Microstructure characterizations and strengthening mechanism of multi-principal component AlCoCrFeNiTi_{0.5} solid solution alloy with excellent mechanical properties, *Mater. Lett.*, 62(2008), p. 2673.
- [4] Y.F. Kao, S.K. Chen, T.J. Chen, P.C. Chu, J.W. Yeh, and S.J. Lin, Electrical, magnetic, and Hall properties of Al_xCoCrFeNi high-entropy alloys, *J. Alloys Compd.*, 509(2011), p. 1607.
- [5] O.N. Senkov, J.M. Scott, S.V. Senkova, D.B. Miracle, and C.F. Woodward, Microstructure and room temperature properties of a high-entropy TaNbHfZrTi alloy, *J. Alloys Compd.*, 509(2011), p. 6043.
- [6] Y.P. Wang, B.S. Li, and H.Z. Fu, Solid solution or intermetallics in a high-entropy alloy, *Adv. Eng. Mater.*, 11(2009), p. 641.
- [7] Y. Zhang, T.T. Zuo, W.B. Liao, and P.K. Liaw, Processing and properties of high-entropy alloys and micro- and nano-wires, *ECS Trans.*, 41(2012), No. 30, p. 49.
- [8] G.J. Wang, B.Q. Xiong, Y.A. Zhang, Z.H. Li, and P.Y. Li, Microstructural characterization of as-cast and homogenized 2D70 aluminum alloy, *Int. J. Miner., Metall. Mater.*, 16(2009), p. 427.
- [9] J.W. Yeh, Y.L. Chen, S.J. Lin, and S.K. Chen, High-entropy alloys: a new era of exploitation, *Mater. Sci. Forum*, 560(2007), p. 1.
- [10] J.W. Yeh, Recent progress in high-entropy alloys, *Ann. Chim. Sci. Mater.*, 31(2006), p. 633.
- [11] L.M. Martyushev and V.D. Seleznev, Maximum entropy production principle in physics, chemistry and biology, *Phys. Rep.*, 426(2006), p. 1.
- [12] Y. Zhang, Y.J. Zhou, J.P. Lin, G.L. Chen, and P.K. Liaw, Solid-solution phase formation rules for multi-component alloys, *Adv. Eng. Mater.*, 10(2008), p. 534.
- [13] X. Yang and Y. Zhang, Prediction of high-entropy stabilized solid-solution in multi-component alloys, *Mater. Chem. Phys.*, 132(2012), p. 233.
- [14] S. Guo, C. Ng, J. Lu, and C.T. Liu, Effect of valence electron concentration on stability of fcc or bcc phase in high entropy alloys, *J. Appl. Phys.*, 109(2011), art. No. 103505.
- [15] Y.L. Chen, C.W. Tsai, C.C. Juan, M.H. Chuang, J.W. Yeh, T.S. Chin, and S.K. Chen, Amorphization of equimolar alloys with HCP elements during mechanical alloying, *J. Alloys Compd.*, 506(2010), p. 210.
- [16] V. Dolique, A.L. Thomann, P. Brault, Y. Tessier, and P. Gillon, Complex structure/composition relationship in thin films of AlCoCrCuFeNi high entropy alloy, *Mater. Chem. Phys.*, 117(2009), p. 142.
- [17] S. Varalakshmi, M. Kamaraj, and B.S. Murty, Formation and stability of equiatomic and nonequiatomic nanocrystalline CuNiCoZnAlTi high-entropy alloys by mechanical alloying, *Metall. Mater. Trans. A*, 41(2010), p. 2703.

- [18] F.J. Wang, Y. Zhang, G.L. Chen, and H.A. Davies, Cooling rate and size effect on the microstructure and mechanical properties of AlCoCrFeNi high entropy alloy, *J. Eng. Mater. Technol.*, 131(2009), No. 3, art. No. 034501.
- [19] C.M. Lin and H.L. Tsai, Evolution of microstructure, hardness, and corrosion properties of high-entropy Al_{0.5}CoCrFeNi alloy, *Intermetallics*, 19(2011), p. 288.
- [20] Y.C. Lin and Y.H. Cho, Elucidating the microstructure and wear behavior for multicomponent alloy clad layers by in situ synthesis, *Surf. Coat. Technol.*, 202(2008), p. 4666.
- [21] O.N. Senkov, G.B. Wilks, D.B. Miracle, C.P. Chuang, and P.K. Liaw, Refractory high-entropy alloys, *Intermetallics*, 18(2010), p. 1758.
- [22] T.T. Shun and Y.C. Du, Microstructure and tensile behaviors of FCC Al_{0.3}CoCrFeNi high entropy alloy, *J. Alloys Compd.*, 479(2009), No. 1-2, p. 157.
- [23] C.W. Tsai, Y.L. Chen, M.H. Tsai, J.W. Yeh, T.T. Shun, and S.K. Chen, Deformation and annealing behaviors of high-entropy alloy Al_{0.5}CoCrCuFeNi, *J. Alloys Compd.*, 486(2009), p. 427.
- [24] J.W. Qiao, S.G. Ma, E.W. Huang, C.P. Chuang, P.K. Liaw, and Y. Zhang, Microstructural characteristics and mechanical behaviors of AlCoCrFeNi high-entropy alloys at ambient and cryogenic temperatures, *Mater. Sci. Forum*, 688(2011), p. 419.
- [25] Y. Zhang, T.T. Zuo, Y.Q. Cheng, and P.K. Liaw, High-entropy alloys with high saturation magnetization, electrical resistivity, and malleability, *Sci. Rep.*, 3(2013), p. 1455.
- [26] O.N. Senkov, G.B. Wilks, J.M. Scott, and D.B. Miracle, Mechanical properties of Nb₂₅Mo₂₅Ta₂₅W₂₅ and V₂₀Nb₂₀Mo₂₀Ta₂₀W₂₀ refractory high entropy alloys, *Intermetallics*, 19(2011), No. 5, p. 698.
- [27] Y. Zhang, X.F. Wang, G.L. Chen, and Y. Qiao, Effect of Ti on the microstructure and properties of CoCrCuFeNiTi_x high-entropy alloys, *Ann. Chim. Sci. Mater.*, 31(2006), No. 6, p. 699.
- [28] X.F. Wang, Y. Zhang, Y. Qiao, and G.L. Chen, Novel microstructure and properties of multicomponent CoCrCuFeNiTi_x alloys, *Intermetallics*, 15(2007), p. 357.
- [29] K.B. Zhang, Z.Y. Fu, J.Y. Zhang, J. Shi, W.M. Wang, H. Wang, Y.C. Wang, and Q.J. Zhang, Annealing on the structure and properties evolution of the CoCrFeNiCuAl high-entropy alloy, *J. Alloys Compd.*, 502(2010), p. 295.
- [30] C. Ng, S. Guo, J.H. Luan, S.Q. Shi, and C.T. Liu, Entropy-driven phase stability and slow diffusion kinetics in an Al_{0.5}CoCrCuFeNi high entropy alloy, *Intermetallics*, 31(2012), p. 165.
- [31] D.L. Shu, J.B. Chen, and Y. Feng, *Mechanical Properties of Engineering Materials*, China Machine Press, Beijing, 2003, p. 43.
- [32] G.F. Sun and W.J. Qiang, *Magnetic Materials*, Chemical Industry Press, Beijing, 2007, p. 2.
- [33] C.J. Qiu, Y.H. Wang, and W. Qu, *Physical Properties of Materials*, Harbin Institute of Technology Press, Harbin, 2009, p. 120.